PCCP

Electron leakage through heterogeneous LiF on lithium-metal battery anodes

Journal:	*Physical Chemistry Chemical Physics*
Manuscript ID	CP-COM-12-2020-006310.R1
Article Type:	Communication
Date Submitted by the Author:	18-Jan-2021
Complete List of Authors:	Smeu, Manuel ; Binghamton University, Physics Leung, Kevin; Sandia National Laboratories, Surface and Interface Science

Journal Name

ARTICLE TYPE

Cite this: DOI: 00.0000/xxxxxxxxxx

Electron leakage through heterogeneous LiF on lithium-metal battery anodes†

Manuel Smeu,*[a] and Kevin Leung,[b]

Received Date
Accepted Date

DOI: 00.0000/xxxxxxxxxx

The solid-electrolyte interphase (SEI) that forms on lithium ion battery (LIB) anodes prevents degradation-causing transfer of electrons to the electrolyte. Grain boundaries (GBs) between different SEI components, like LiF, have been suggested to accelerate Li^+ transport. However, using the non-equilibrium Green's function technique with density functional theory (NEGF-DFT), we find that GBs enhance electron tunneling in thin LiF films by 1-2 orders of magnitude, depending on the bias. Extrapolating to thicker films using the Wentzel-Kramers-Brillouin (WKB) method emphasizes that safer batteries require passivation of GBs in the SEI.

Reliable energy storage is one of the most pressing issues in electrification of transportation, implementation of renewable energy sources into the grid, and the continued demand for consumer electronics.[1] In secondary (rechargeable) batteries, the active ions (*e.g.*, Li ions) will shuttle between the anode and the cathode through the electrolyte. The charge is compensated by electrons shuttling between the anode and the cathode via the external circuit. In other words, the electrolyte needs to be highly conductive to ions while being insulating to electrons.

As the electrolyte comes in direct contact with the anode/cathode, or under the action of long-range electron transfer,[2] electrons move to/from the former, thereby reducing/oxidizing it and resulting in electrolyte decomposition. This is managed by the formation of the solid-electrolyte interphase (SEI) or cathode-electrolyte interphase (CEI) layer. The SEI/CEI is a complex agglomeration of decomposed electrolyte species that deposit on the anode/cathode forming a passivation layer, with cross-talk possible.[3] We focus on the anode.

The region of SEI closer to the anode is typically made up of inorganic compounds, while the region closer to the electrolyte is made up of organic compounds.[4] This layered structure is in fact inevitable for reactive anodes like Li metal, which reacts with organic SEI components.[5] Since the SEI is made up of a multitude of chemical compounds, there is great variability in its ability to protect the anode and electrolyte from degradation, which is not yet well understood. In particular, the solid-solid interfaces between different inorganic SEI components have been suggested to enhance Li^+ transport,[6–9] but their electron leakage properties have not been explored. This provides the impetus for fundamental studies to understand the structure-electron blockage function relationships of the SEI components, defects, and interfaces, and facilitate the rational design of advanced batteries.

Some measurements of the aggregate electronic resistivity of composite SEI films have been reported.[10,11] Theoretical understanding of the conductivity contribution from individual SEI components will help interpret such data. 4-5 nm thick, defect-free crystalline inorganic SEI films have been predicted to stop electron tunneling.[2,12] However, SEI interfaces, extended defects, and grain boundaries (GBs) may drastically reduce passivation capability. For example, artificially grown SEI components like LiF, known to be a good insulator,[13] yield less-than-ideal passivating properties due to the microstructure.[14] Lithium dendrites are known to materialize inside pores and cracks of ceramic solid electrolytes.[15]

Computationally, lithium metal atoms and clusters have been predicted to form at LiF and Li_2O GBs,[16] inducing passivation breakdown via lithium diffusion. Another mechanism commonly associated with electron leakage is ballistic "tunneling" through homogeneous SEI model films. The tunneling probability as the SEI thickness varies has been estimated using the Wentzel-Kramers-Brillouin (WKB) approximation.[2,12] However, WKB is not designed to deal with SEI inhomogeneities discussed earlier, especially extended defects like GBs. The non-equilibrium

[a] *Department of Physics, Binghamton University - SUNY, Binghamton, NY 13902, USA. E-mail: msmeu@binghamton.edu*

[b] *Sandia National Laboratories, MS 1415, Albuquerque, NM 87185, USA.*

† Electronic Supplementary Information (ESI) available: Comparative transmission spectra for Li with various amounts of strain; description of how the two-probe Li–LiF–Li structures are generated, *I-V* plot obtained at lower precision comparing systems without and with GBs for a wider voltage window, local density of states for Li–LiF–Li systems without and with GBs, transmission ratios with GBs vs. without GBs obtained with the NEGF-DFT and WKB methods. See DOI: 00.0000/00000000.

Green's Function coupled with Density Functional Theory (NEGF-DFT) technique, while computationally expensive, is the method of choice to predict electron transport through media with atomic-length scale inhomogeneities.[17] So far, NEGF has been applied to study electron conductivity through electrolyte molecules and nanocrystals of SEI components.[18,19] These have been proof-of-principle calculations; the SEI film is a dense solid, not a cluster residing in vacuum, and if excess e^- reaches a solvent molecule, the latter would be reductively decomposed. The present work builds off of these advances, culminating in in a formalism and a prototype model that arguably lays the foundation for quantitative studies of electron leakage through SEI defects.

We employ state-of-the-art NEGF-DFT to calculate the electronic conductance through GBs that connect LiF grains [Fig. 1(c,d)]. Our approach advances the field beyond what has been done in the following ways. *i*) The NEGF-DFT method allows us to obtain the non-equilibrium (current-voltage) electron transport characteristics. *ii*) The models used consist of bulk systems rather than isolated molecules/nanostructures, which are more representative of an SEI environment. *iii*) The effects of inhomogeneities (GBs) on the conductivity of SEI components[16] are investigated in systems with up to 1,000 atoms. Although the SEI films that can be represented at this size remain thin (on the order of 10 Å), this computational approach represents the most promising method to make quantative contact with measurements. By comparing two systems sandwiched between metal Li electrodes and calculating the electrical conductance, one with GBs and the other with pristine LiF, we highlight the importance of defects in SEI passivation breakdown and make contact with WKB theory, which has been applied previously in this field.

The LiF crystal was prepared in the rocksalt crystal structure and fully relaxed with the Vienna *ab initio* simulation package (VASP).[20,21] We used the projector augmented wave potentials[22] with the Perdew-Burke-Enerzerhof generalized gradient approximation (PBE-GGA).[23] The energy cutoff was 500 eV and the cells employed sufficient *k*-points for the energy to be converged within 1 meV/atom. The relaxations were continued until forces on atoms were less than 0.02 eV/Å. We have not calculated the electronic voltage of this system; however, previous DFT modeling of lithium metal/LiF (001) interfaces, with and without GBs, are found to exhibit nearly 0.0 V vs. Li^+/Li(s) without the need to impose additional electric double layers.[16]

Since LiF is harder than Li, the two-probe structures were built such that the LiF preserved its crystal structure (with a lattice constant of 4.11 Å) while the Li was strained to accommodate the lattice mismatch.[24] The strain along any axis in either system (with and without GBs) was less than 1% *. The two-probe structures in Fig. 1 were built by first relaxing a periodic structure containing (strained) crystalline Li and crystalline LiF separated by an intermediate Li region, and then extending the crystalline Li to form semi-infinite electrodes to the left and right of the LiF region (see Fig. S2 and corresponding text, ESI†). The GB-containing LiF system is based on a structure from the literature.[13,16]

We calculate the electronic conductance using the NEGF-DFT code Nanodcal.[25,26] A central construct in NEGF-DFT is the retarded Green's function,

$$G(E) = [ES - H - \Sigma_L - \Sigma_R]^{-1}, \quad (1)$$

where H and S are the Hamiltonian and overlap matrices for the central region of the two-probe structure, calculated by DFT. $\Sigma_{L,R}$ are self-energies that account for the effect of the left/right electrodes on the central region; these are complex quantities with their real part representing a shift in the energy levels and their imaginary part representing the broadening, which can also be represented as the linewidth matrix, $\Gamma_{L,R} = i(\Sigma_{L,R} - \Sigma_{L,R}^\dagger)$. The self-energy is calculated within the NEGF-DFT formalism by an iterative technique.[27] The electronic density matrix can be calculated from these quantities as,

$$\rho = \frac{1}{2\pi}\int_{-\infty}^{\infty}[f(E,\mu_L)G\Gamma_L G^\dagger + f(E,\mu_R)G\Gamma_R G^\dagger]dE, \quad (2)$$

where $\mu_{L,R}$ are the electrochemical potentials of the left and right electrodes and the Fermi-Dirac function describes the probability of occupying a single-particle orbital with a given energy at a specified electrochemical potential. The bias voltage between the two electrodes is given by, $eV_b = \mu_L - \mu_R$. The density obtained from the above equation is used in a subsequent NEGF-DFT iteration step and the cycle is repeated until self-consistency is achieved in terms of the Hamiltonian and electron density. The transmission function is then obtained from the Green's function,

$$T(E,V_b) = \mathrm{Tr}(\Gamma_L G \Gamma_R G^\dagger), \quad (3)$$

which represents the probability that an electron with a given energy, E, transmits from one electrode through the central region into the other electrode. The current for a given bias, V_b, can then be calculated with the Landauer-Büttiker equation[28],

$$I(V_b) = \frac{2e}{h}\int_{-\infty}^{\infty} T(E,V_b)[f(E,\mu_L) - f(E,\mu_R)]dE. \quad (4)$$

The transmission spectra, $T(E)$, for the two Li–LiF–Li systems without and with GBs are shown in Fig. 2(a) and 2(b) on linear and logarithmic scales, respectively. Both LiF systems are insulating to electron transport, having band gaps larger than 4 eV and 3 eV for the pristine LiF and the LiF with GBs, respectively. This is manifested by the low transmission near the Fermi level, E_F, of the Li metal electrodes [dashed line in Fig. 2(a)]. However, the system with GBs has its conduction band at a lower energy, resulting in a larger transmission function tail passing through E_F, which can be seen when plotting transmission on a logarithmic scale [Fig. 2(b)]. The conductance of the pristine LiF is 4.35×10^{-5} G_0 while that of the LiF with GBs is greater by more than one order of magnitude, 8.28×10^{-4} G_0 ($G_0 = 2e^2/h \approx 77.5$ μS, the quantum of conductance). Note that these quantities are normalized to the lateral cross section of each system. It should be pointed out that these NEGF-DFT calculations are affected by the known limitations of PBE/DFT, namely

* Note that this strain on the Li did not appreciably affect its electrical conductance properties. We tested the conductance of strained vs. unstrained Li, which gave nearly identical results (See Fig. S1, ESI†).

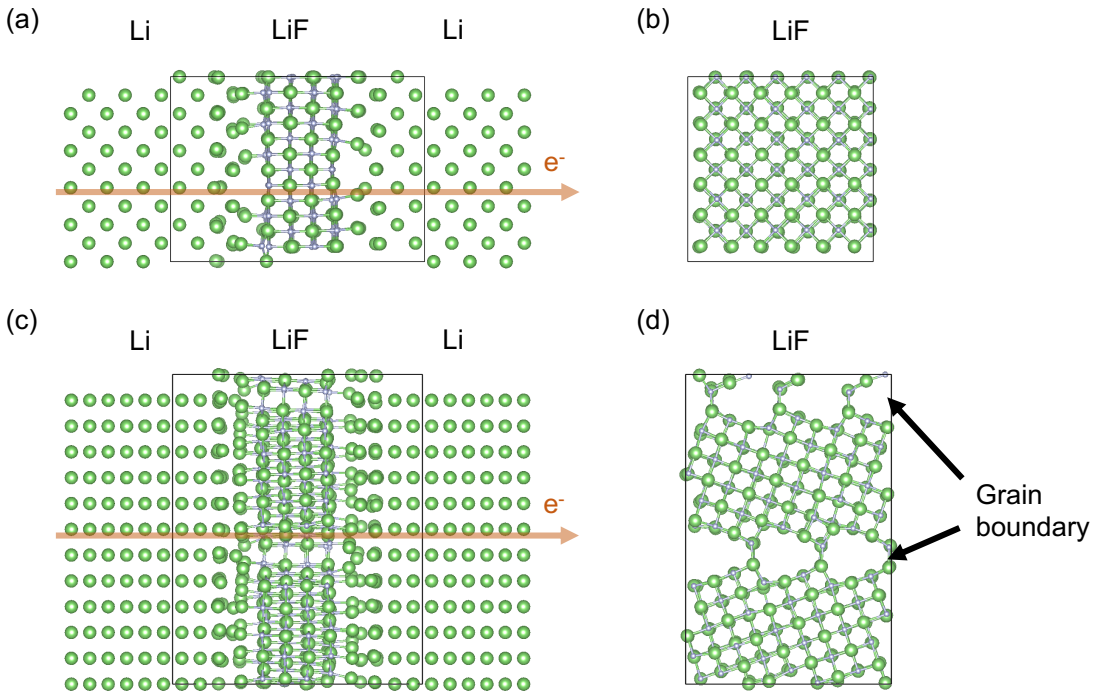

Fig. 1 LiF structures considered in this work sandwiched between Li metal electrodes. (a) Side and (b) end views of pristine LiF; (c) side and (d) end views of two LiF grains separated by grain boundaries. The LiF regions are 2D periodic in the plane perpendicular to the electron transport direction (orange arrow).

the band gap being underestimated. However, we have found that excellent agreement with experiment can still be obtained when relative comparisons are made,[17,29–33] which is the approach taken in the present work.

To get a better insight into this result, the real space scattering states are investigated. These represent the wave function of an electron as it transmits (tunnels) through the central region from one electrode to the other. The scattering states at 1.7 eV are plotted for the pristine LiF and LiF with GBs in Fig. 2(c) and 2(d), respectively. For the pristine LiF [Fig. 2(c)], the scattering state does not penetrate through the LiF, meaning the electrons do not tunnel well through this barrier. In contrast, the LiF with GBs [Fig. 2(d)] has scattering states that extend through the LiF region, permitting electrons to tunnel from one Li electrode to the other, through the LiF. It is noteworthy that the scattering state follows the GB, which reveals the path of least resistance in these systems.

We next consider the non-equilibrium electron transport properties of the LiF systems. We emphasize that such calculations, away from zero bias, are unique to NEGF. The current-voltage (*I-V*) relationship was calculated using Eq. 4 and is shown in Fig. 3. As expected, the system with the GBs (heterogeneities) would conduct nearly two orders of magnitude more current at a given bias compared to the pristine (single-crystal) LiF system. It is interesting to note that, at low bias, the *I-V* characteristics are linear, though they drastically increase at voltages greater than 2 V, corresponding to the inclusion of the conduction band in the bias window (see Fig. S3, ESI†). In battery terms, a positive bias corresponds to a voltage negative of 0.0 V vs. $Li^+/Li(s)$, which is seen to strongly enhance electron leakage through this model SEI.

A GB-enhancement of transmission coefficient of two orders of magnitude would not strongly affect e^- blocking properties if the surface density of GB is low. However, this enhancement was computed for a ~10 Å thick LiF film. To effectively block electrons, inorganic, crystalline SEI films need to be > 4 nm thick.[2] Since such system sizes are not currently accessible with NEGF-DFT, we next apply the simplified WKB approximation used in Ref. 2 to extrapolate e^- leakage in thicker films:

$$k_t \propto \exp[-2\sqrt{2m_e(E_{offset}-V_b)}R/\hbar]. \quad (5)$$

Here k_t is tunneling probability, m_e is the electron mass, E_{offset} is the energy difference between the conduction band edge and the Fermi level, $\hbar$ is Plank's constant divided by 2π, and R is the film thickness.

E_{offset} is estimated from the local density-of-state plot in Fig. S4 (ESI†) which is based on the the highest ΔE in the insulating LiF region; it is 1.63 eV and 2.93 eV with and without the GB, respectively. Fig. S4 also shows that the LiF/Li interfaces are not step-functions electronically speaking. To estimate the effective thickness R, assumed to be the same in both cases, we fit the ratio of transmission coefficients with/without GB as a function of the applied bias. $R = 6.5$ Å gives a reasonable fit (see Fig. S5, ESI†). With the two sets of $\{R, E_{offset}\}$, Eq. 5 predicts that a 4-nm thick film of LiF with GBs would have a conductance 5.5×10^7 times greater than pristine LiF of the same dimensions at $V_{bias}=0$ V. This rises to a factor of 4.0×10^9 at $V_{bias}=1$ V. While these are order-of-magnitude estimates, they emphasize that even a low GB den-

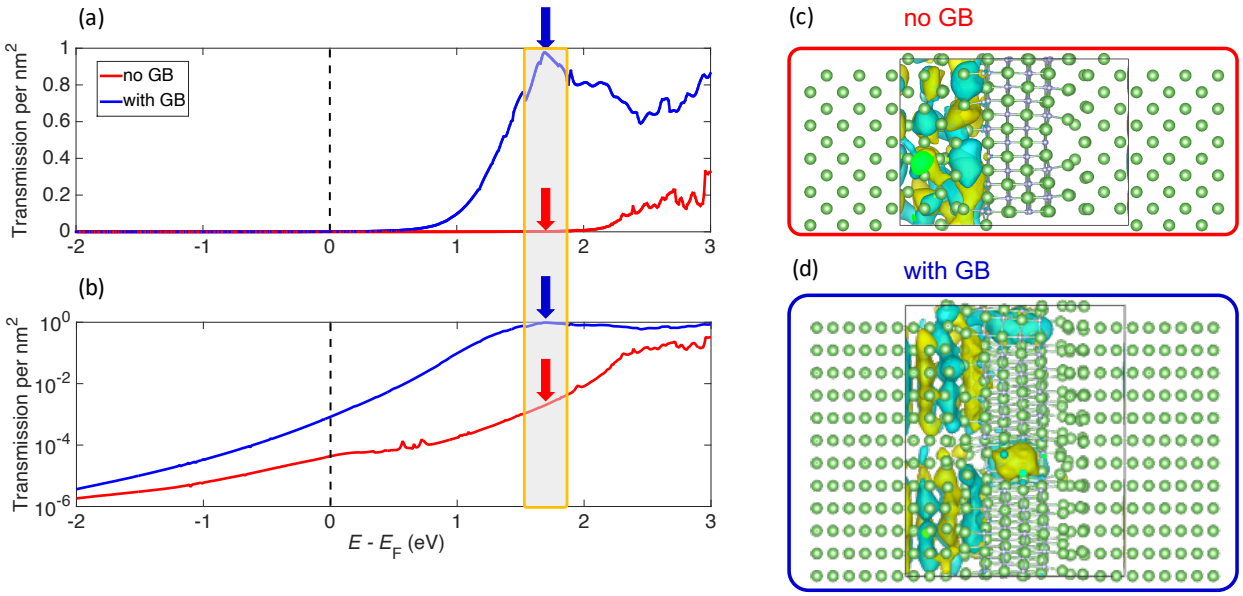

Fig. 2 Transmission spectra of the LiF systems on (a) linear and (b) logarithmic scales. The red and blue arrows illustrate the transmission at 1.7 eV for the LiF without and with grain boundaries, respectively. The scattering states at 1.7 eV are plotted in real space for these systems in (c) and (d).

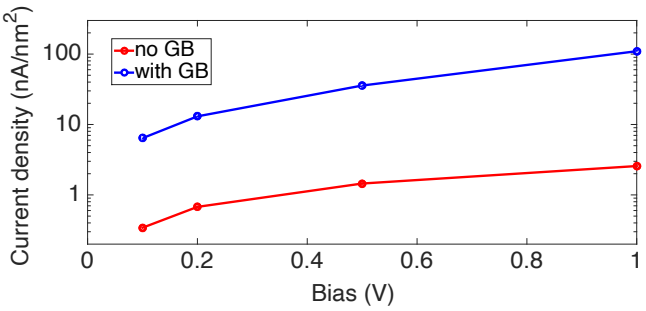

Fig. 3 Current density as a function of bias voltage for LiF without and with grain boundaries.

sity is sufficient to significantly degrade the e^- blocking property of SEI films when accounting for the reduced capacity of GBs to prevent electron transport. Note that Ref. 16 considered only Li atom transport as a way of electron leakage, and found that this mode of electron leakage works for grain boundaries in Li_2O but not LiF because LiF is a "negative electron affinity" material. We concluded that LiF is a good SEI component for electron blocking even if it has extended defects in Ref. 16. The present work shows that that conclusion was premature because we did not consider ballistic electron transport through these defects, which greatly enhance leakage through LiF grain boundaries. Therefore, for a given surface area of LiF, the presence of defects such as grain boundaries would dramatically increase the rate of electrolyte decomposition compared to pristine (defect-free) LiF.

In the future, our NEGF approach should be extended to thicker SEI films and different defect structures, and phonon dissipation terms should be included, to obtain predictions of SEI e^- blocking properties more quantitative than is possible with the WKB method. Additionally, this analysis can be applied to the multitude of other SEI components, which include other inorganic (*e.g.*, Li_2O) as well as organic (*e.g.*, lithium ethylene decarbonate) species. This work highlights the importance of developing next-generation NEGF codes for battery applications.

In conclusion, we performed large-scale NEGF-DFT electron transport calculations on GBs in LiF, which are models for extended defects in lithium-metal-passivating SEI films in lithium ion batteries. Pristine (single crystal) LiF was also considered to provide comparison. While both systems were about 1 nm thick and were insulating, the LiF with GBs was an order of magnitude more conductive than the pristine system. Scattering state analysis confirms that the electrons can effectively leak along the GBs. Using the WKB approximation, parameterized DFT band alignment and NEGF calculations, the GB region is found to exhibit conductance 7-9 orders of magnitude higher than pristine LiF in what would be an inorganic SEI thickness of at least 4 nm. These results highlight the important role that heterogeneities can play in the performance of the SEI during battery operation, and provide insights into how current leakage can be mitigated. They pave the way for future investigation of other grain boundaries and defects in other SEI materials, and inclusion of dissipation effects.

Conflicts of interest

There are no conflicts to declare.

Acknowledgements

KL thanks Andrew Baczewski for useful suggestions. MS was funded by Nanostructures for Electrical Energy Storage (NEES), an Energy Frontier Research Center funded by the U.S. Department of Energy, Office of Science, Office of Basic Energy Sciences under Award Number DESC0001160. KL was supported by Sandia Laboratory Directed Research and Development (LDRD)

project 218253. Sandia National Laboratories is a multi-mission laboratory managed and operated by National Technology and Engineering Solutions of Sandia, LLC., a wholly owned subsidiary of Honeywell International, Inc., for the U.S. Department of Energy's National Nuclear Security Administration under contract DE-NA-0003525. This paper describes objective technical results and analysis. Any subjective views or opinions that might be expressed in the paper do not necessarily represent the views of the U.S. Department of Energy or the United States Government.

Notes and references

1 J. Liu, Z. Bao, Y. Cui, E. J. Dufek, J. B. Goodenough, P. Khalifah, Q. Li, B. Y. Liaw, P. Liu, A. Manthiram, Y. S. Meng, V. R. Subramanian, M. F. Toney, V. V. Viswanathan, M. S. Whittingham, J. Xiao, W. Xu, J. Yang, X. Q. Yang and J. G. Zhang, *Nat. Energy*, 2019, **4**, 180–186.
2 K. Leung, Y. Qi, K. R. Zavadil, Y. S. Jung, A. C. Dillon, A. S. Cavanagh, S.-H. Lee and S. M. George, *J. Am. Chem. Soc.*, 2011, **133**, 14741–14754.
3 R. Sahore, F. Dogan and I. D. Bloom, *Chem. Mater.*, 2019, **31**, 2884–2891.
4 A. Schechter, D. Aurbach and H. Cohen, *Langmuir*, 1999, **15**, 3334–3342.
5 K. Leung, F. Soto, K. Hankins, P. B. Balbuena and K. L. Harrison, *J. Phys. Chem. C*, 2016, **120**, 6302–6313.
6 J. Pan, Q. Zhang, X. Xiao, Y. Cheng and Y. Qi, *ACS Appl. Mater. Interfaces*, 2016, **8**, 5687–5693.
7 R. Xu, C. Yan, Y. Xiao, M. Zhao, H. Yuan and J.-Q. Huang, *Energy Storage Mater.*, 2020, **28**, 401–406.
8 C. Wang, K. Aoyagi, M. Aykol and T. Mueller, *ACS Appl. Mater. Interfaces*, 2020, **12**, 55510–55519.
9 Y. Qi, C. Ban and S. J. Harris, *Joule*, 2020, **4**, 2599–2608.
10 C. Stetson, T. Yoon, J. Coyle, W. Nemeth, M. Young, A. Norman, S. Pylypenko, C. Ban, C.-S. Jiang, M. Al-Jassim and A. Burrell, *Nano Energy*, 2019, **55**, 477 – 485.
11 M. Tang and J. Newman, *J. Electrochem. Soc.*, 2012, **159**, A1922–A1927.
12 Y.-X. Lin, Z. Liu, K. Leung, L.-Q. Chen, P. Lu and Y. Qi, *J. Power Sources*, 2016, **309**, 221–230.
13 K. P. McKenna and A. L. Shluger, *Nat. Mater.*, 2008, **7**, 859–862.
14 M. He, R. Guo, G. M. Hobold, H. Gao and B. M. Gallant, *Proc. Natl. Acad. Sci. U. S. A.*, 2020, **117**, 73–79.
15 E. J. Cheng, A. Sharafi and J. Sakamoto, *Electrochim. Acta*, 2017, **223**, 85–91.
16 K. Leung and K. L. Jungjohann, *J. Phys. Chem. C*, 2017, **121**, 20188–20196.
17 B. V. C. Martins, M. Smeu, L. Livadaru, H. Guo and R. A. Wolkow, *Phys. Rev. Lett.*, 2014, **112**, 246802.
18 L. Benitez, D. Cristancho, J. M. Seminario, J. M. Martinez De La Hoz and P. B. Balbuena, *Electrochim. Acta*, 2014, **140**, 250–257.
19 L. Benitez and J. M. Seminario, *J. Phys. Chem. C*, 2016, **120**, 17978–17988.
20 G. Kresse and J. Hafner, *Phys. Rev. B*, 1993, **47**, 558–561.
21 G. Kresse and J. Furthmüller, *Phys. Rev. B*, 1996, **54**, 11169–11186.
22 P. E. Blöchl, *Phys. Rev. B*, 1994, **50**, 17953–17979.
23 J. P. Perdew, K. Burke and M. Ernzerhof, *Phys. Rev. Lett.*, 1996, **77**, 3865–3868.
24 K. Leung, *Phys. Chem. Chem. Phys.*, 2020, **22**, 10412–10425.
25 J. Taylor, H. Guo and J. Wang, *Phys. Rev. B*, 2001, **63**, 245407.
26 D. Waldron, P. Haney, B. Larade, A. MacDonald and H. Guo, *Phys. Rev. Lett.*, 2006, **96**, 166804.
27 M. P. L. Sancho, J. M. L. Sancho and J. Rubio, *J. Phys. F*, 1984, **14**, 1205–1215.
28 S. Datta, *Electronic transport in mesoscopic systems*, Cambridge University Press, Cambridge, 1995.
29 Z. Li, M. Smeu, M. Ratner and E. Borguet, *J. Phys. Chem. C*, 2013, **117**, 14890—-14898.
30 Z. Li, M. Smeu, S. Afsari, Y. Xing, M. a. Ratner and E. Borguet, *Angew. Chem. Int. Ed.*, 2014, **53**, 1098–1102.
31 Z. Li, M. Smeu, T.-H. Park, J. Rawson, Y. Xing, M. J. Therien, M. a. Ratner and E. Borguet, *Nano Lett.*, 2014, **14**, 5493–9.
32 Z. Li, M. Smeu, A. Rives, V. Maraval, R. Chauvin, M. a. Ratner and E. Borguet, *Nat. Commun.*, 2015, **6**, 6321.
33 P. Yasini, S. Shepard, T. Albrecht, M. Smeu and E. Borguet, *J. Phys. Chem. C*, 2020, **124**, 9460–9469.